Supporting Information

Structure/Interface Cooperative Regulation Stabilizes High-Nickel Cathodes for Lithium-Ion Batteries

Guihong Mao,[ab] Liming Zeng,[a] Jieyu Yang,[b] Tengyu Yao,[b] Fangming Xiao,[a] Renheng Tang,[a] Xin Shu,[c] Ying Wang*[a] and Laifa Shen*[b]

a State Key Laboratory of Rare Metals Separation and Comprehensive Utilization, Guangdong Provincial Key Laboratory of Rare Earth Development and Application, Institute of Resources Utilization and Rare Earth Development, Guangdong Academy of Sciences, Guangzhou 510650, China.

b Jiangsu Key Laboratory of Electrochemical Energy Storage Technologies, College of Material Science and Engineering, Nanjing University of Aeronautics and Astronautics, Nanjing 211106, China.

c Hunan Aerospace TianLu Advanced Material Testing Co., Ltd, Changsha 410000, China.

***Corresponding Authors:** E-mail: wangying@irmgdas.gd.cn (Prof. Ying Wang), lfshen@nuaa.edu.cn (Prof. Laifa Shen)

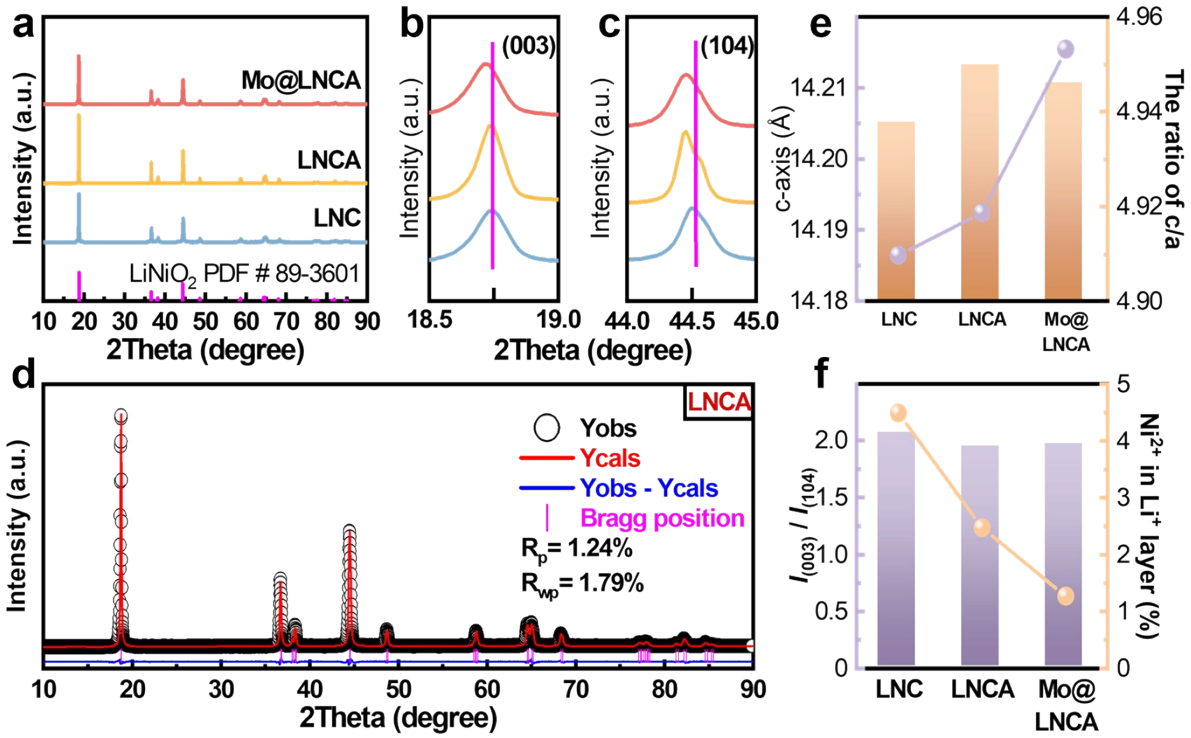

Fig. S1. a) XRD patterns of LNC, LNCA, and Mo@LNCA with enlarged views of b) (003) peaks and c) (104) peak. d) XRD refinement results of LNCA. e) the lattice parameters c and c/a values obtained by the refinement. f) the values of I(003)/I(104) and the proportion of Ni^{2+} in the Li^{+} layer.

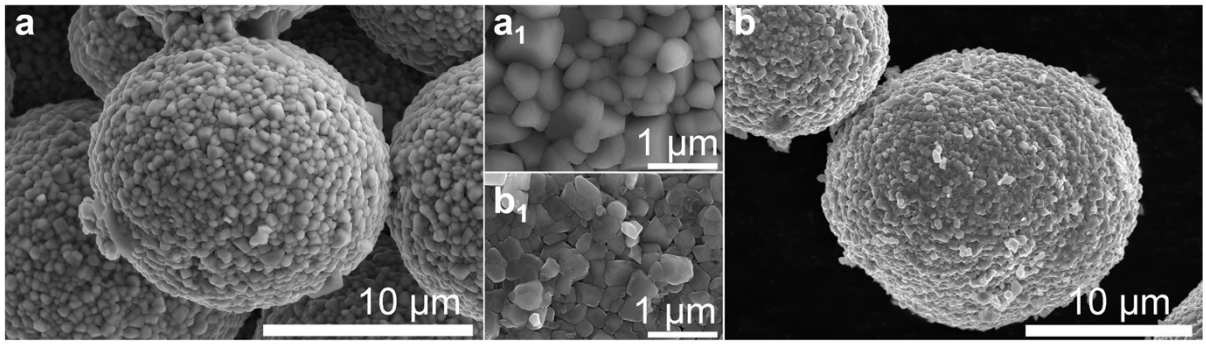

Fig. S2. SEM images of a) LNC and b) LNCA.

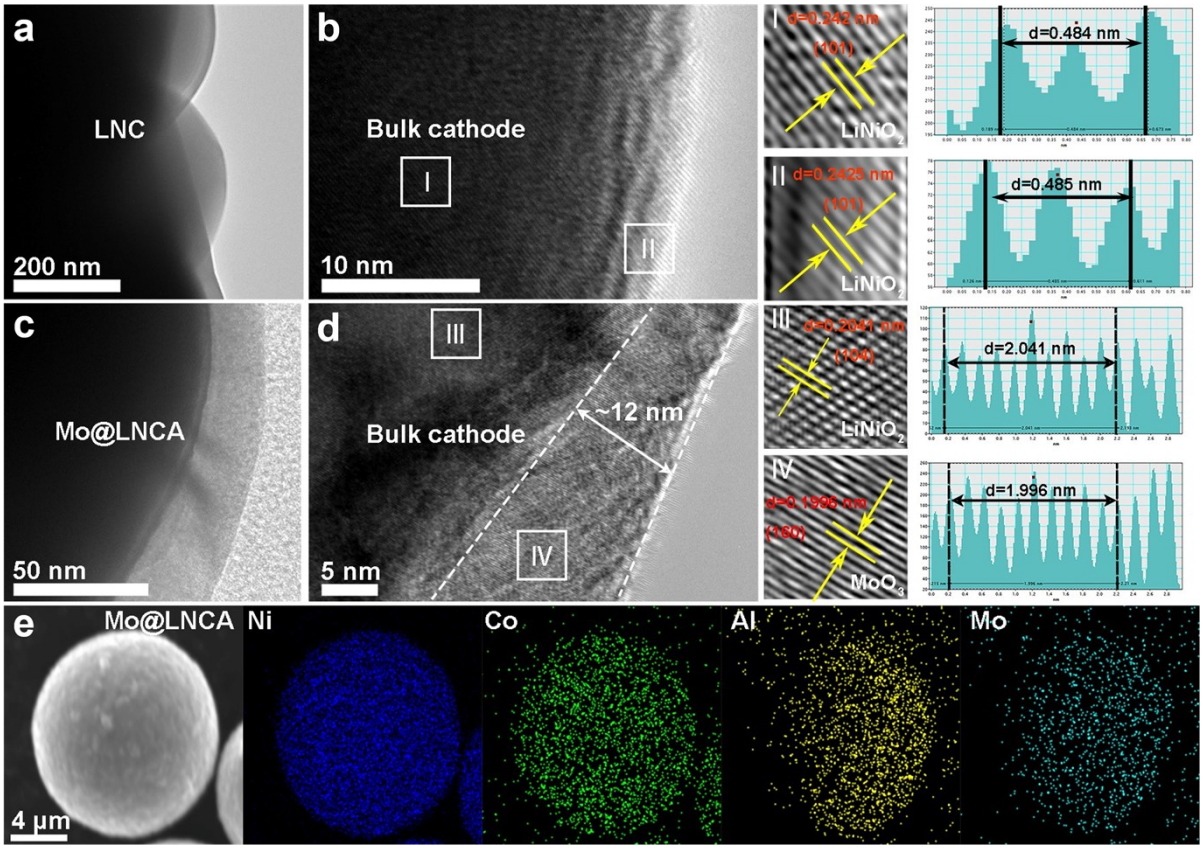

Fig. S3. TEM images of a-b) LNC and c-d) Mo@LNCA. e) EDS mapping of Mo@LNCA.

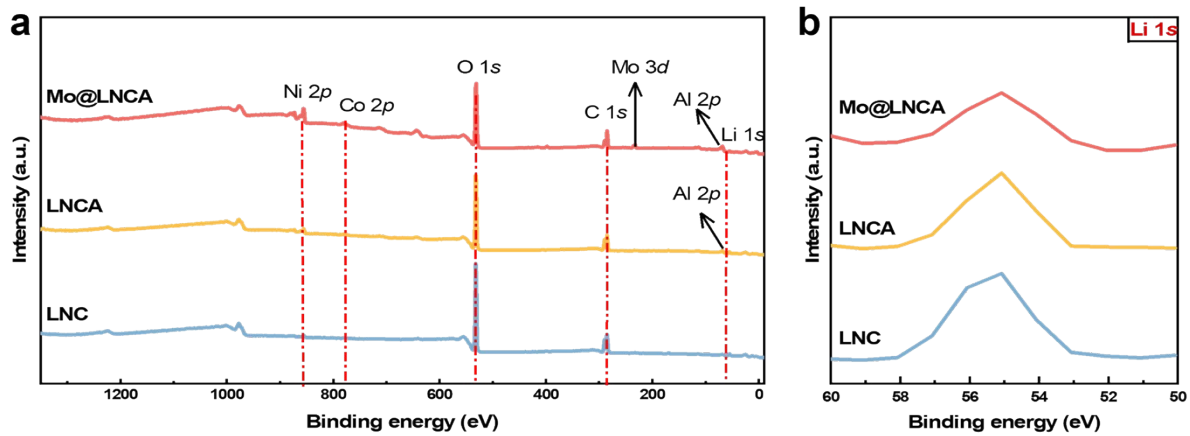

Fig. S4. a) XPS survey spectra and b) the corresponding high-resolution spectra of Li 1*s* of cathode powders.

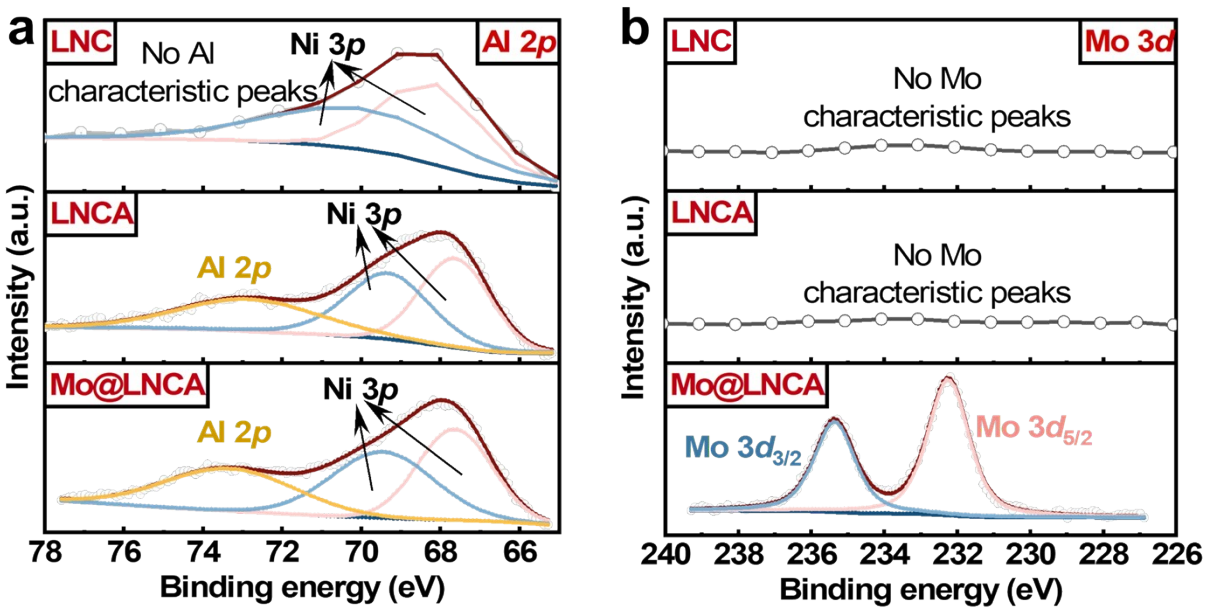

Fig. S5. XPS spectra of a) Al 2*p* and b) Mo 3*d*.

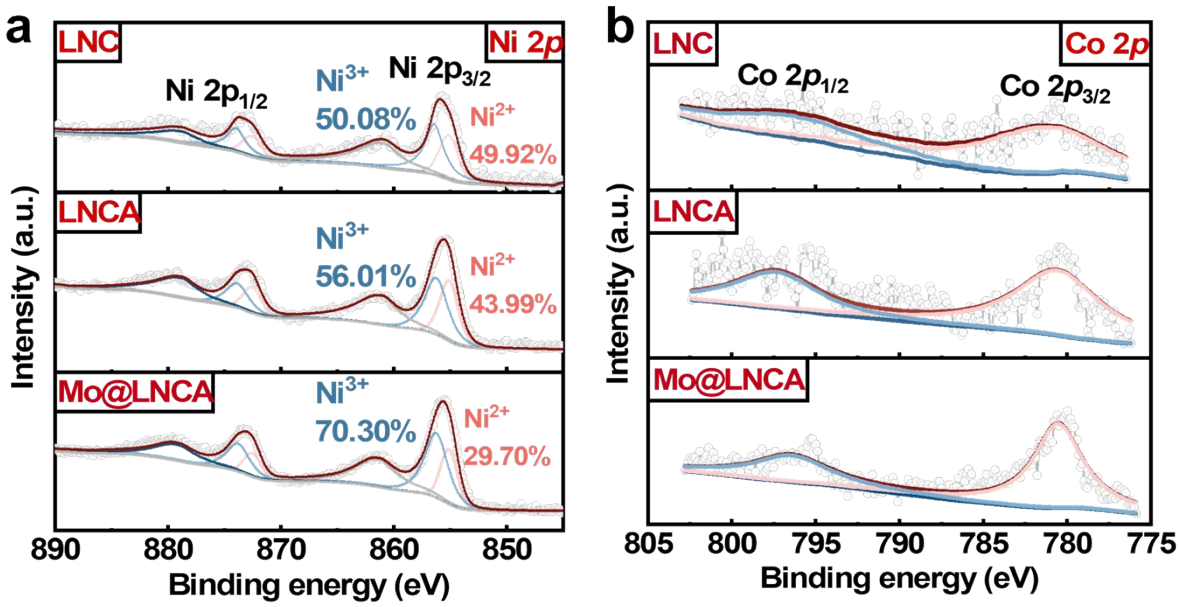

Fig. S6. XPS spectra of a) Ni 2*p* and b) Co 2*p*.

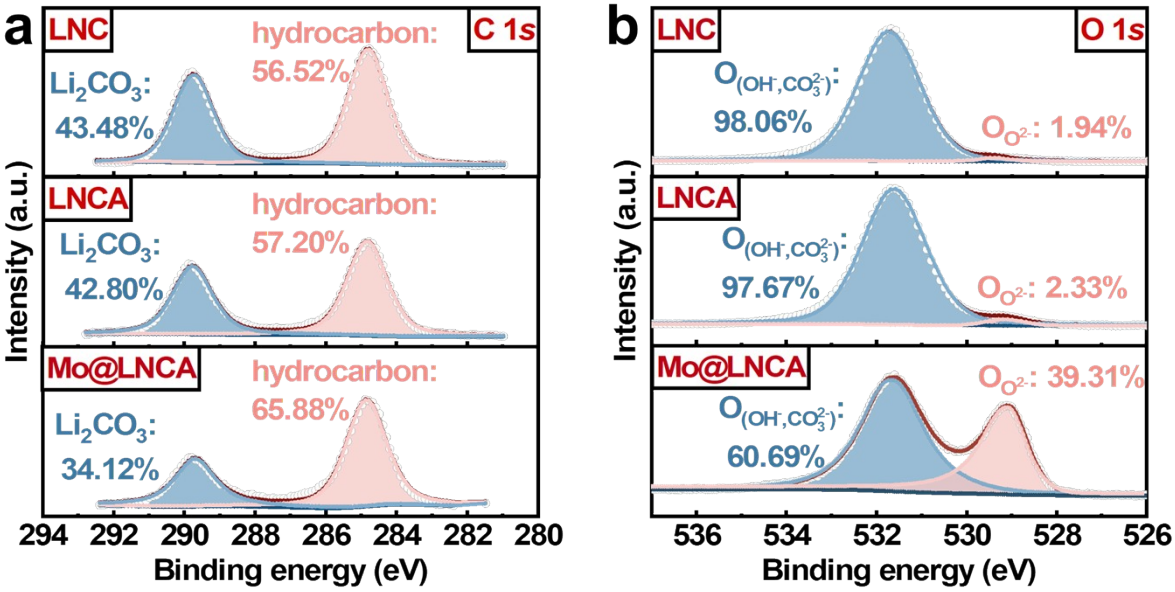

Fig. S7. XPS spectra of a) C 1*s* and b) O 1*s*.

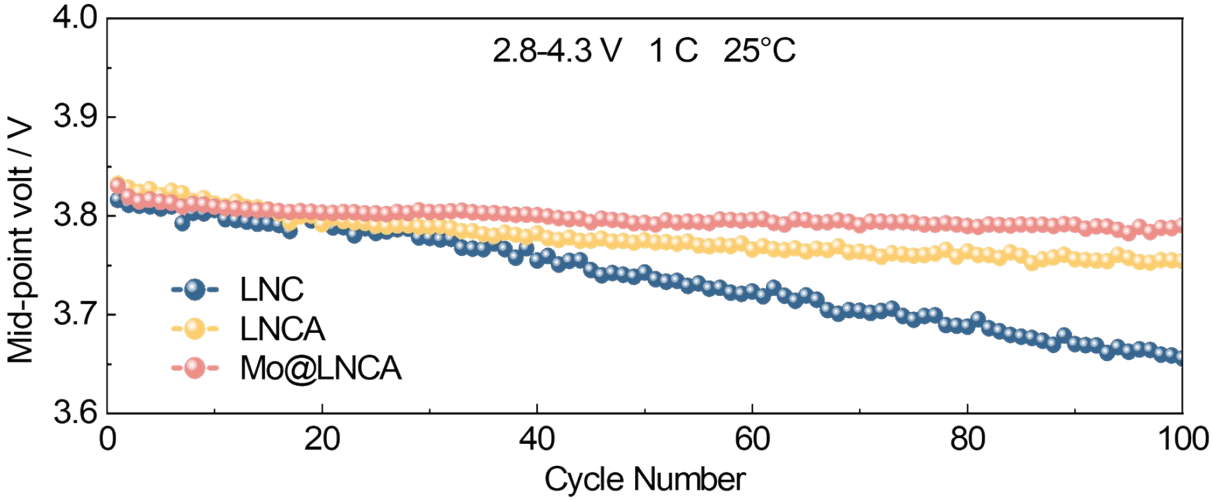

Fig. S8. Median discharge voltage diagram of LNC, LNCA and Mo@LNCA samples.

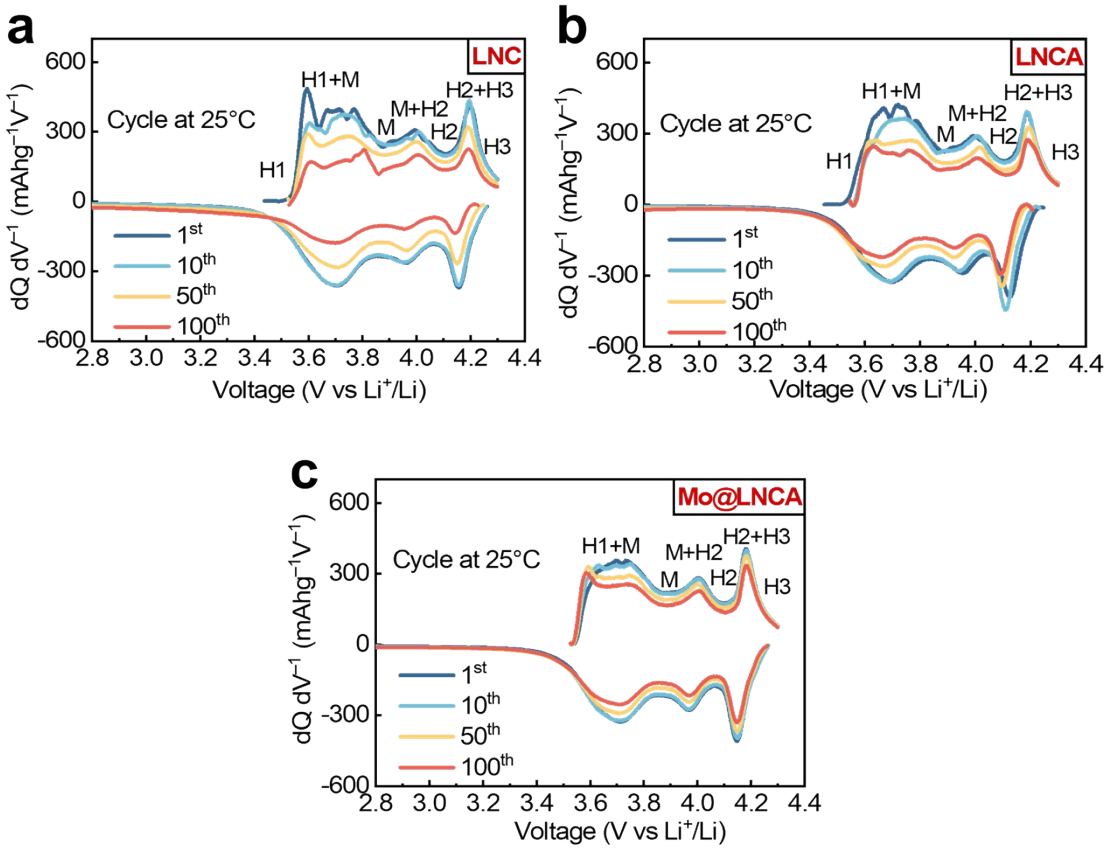

Fig. S9. dQ dV^{-1} curves of the a) LNC, b) LNCA and c) Mo@LNCA at 25°C during the cycle.

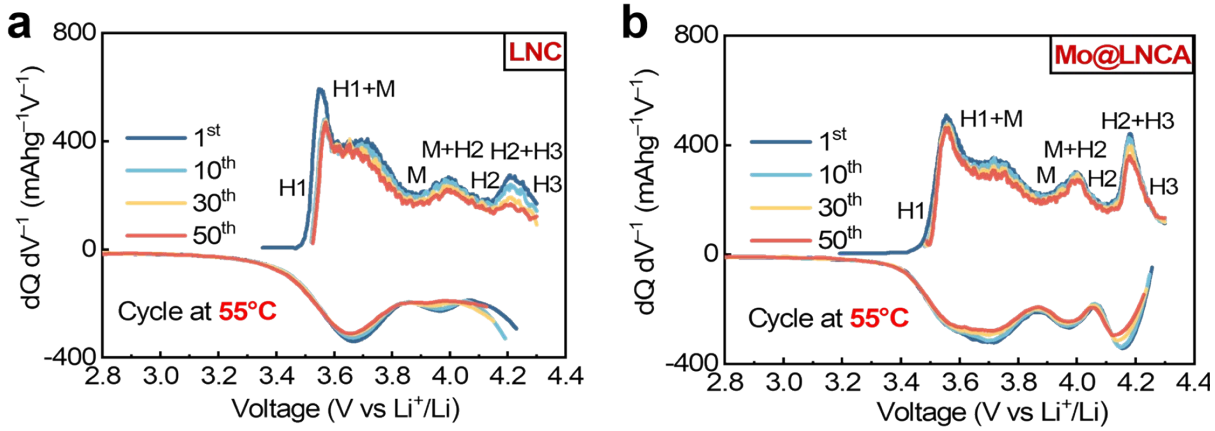

Fig. S10. dQ dV^{-1} curves of the a) LNC and b) Mo@LNCA at 55°C during the cycle.

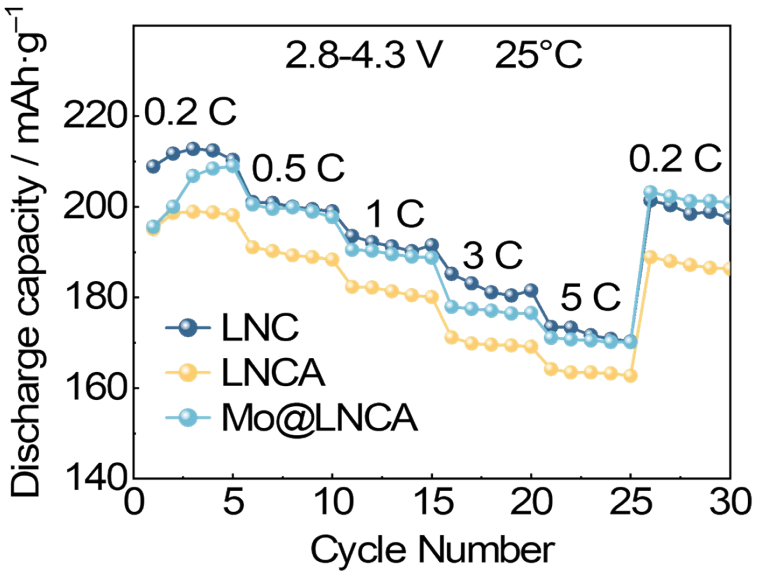

Fig. S11. The rate capability in the range of 2.8−4.3 V at 25°C.

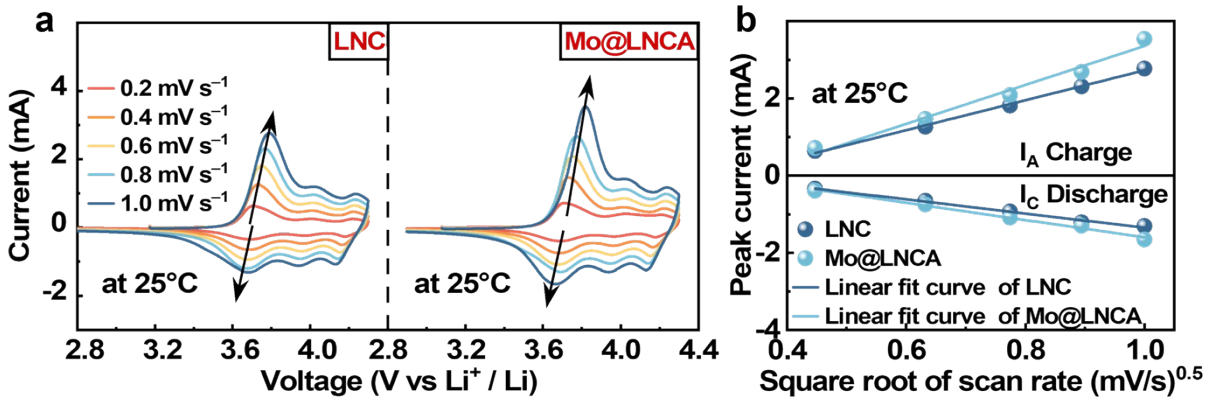

Fig. S12. a) CV curves of LNC and Mo@LNCA at different scanning rates and b) relationship between logarithm anode peak current (Ip) and logarithm scan rates ($V^{1/2}$) of two samples at 25°C

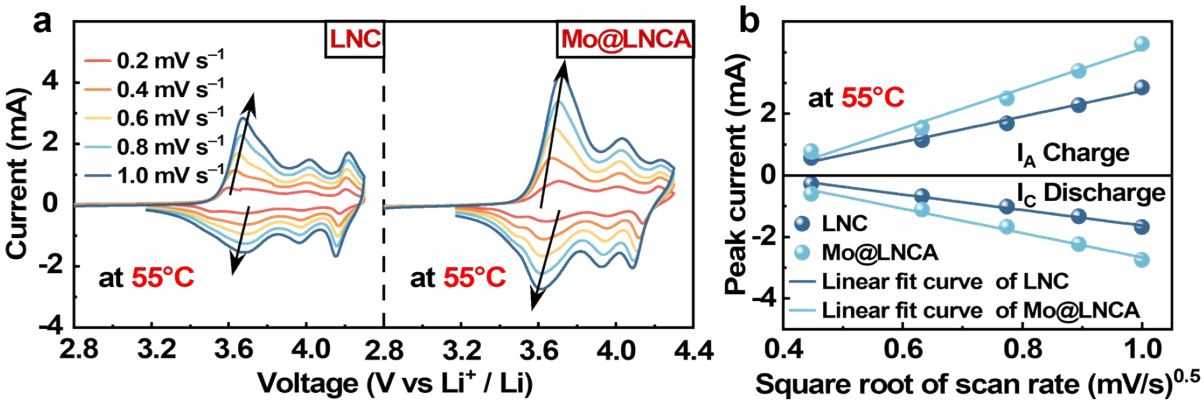

Fig. S13. a) CV curves of LNC and Mo@LNCA at different scanning rates and b) relationship between logarithm anode peak current (Ip) and logarithm scan rates ($V^{1/2}$) of two samples at 55°C.

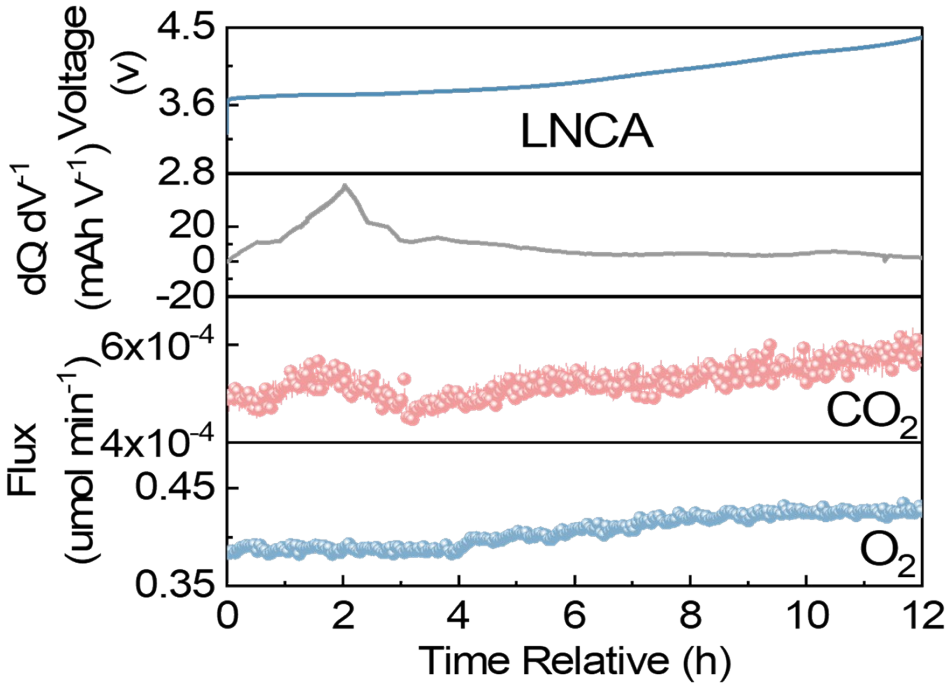

Fig. S14. In situ DEMS measurements for LNCA during charging process to 4.3 V for the first cycle.

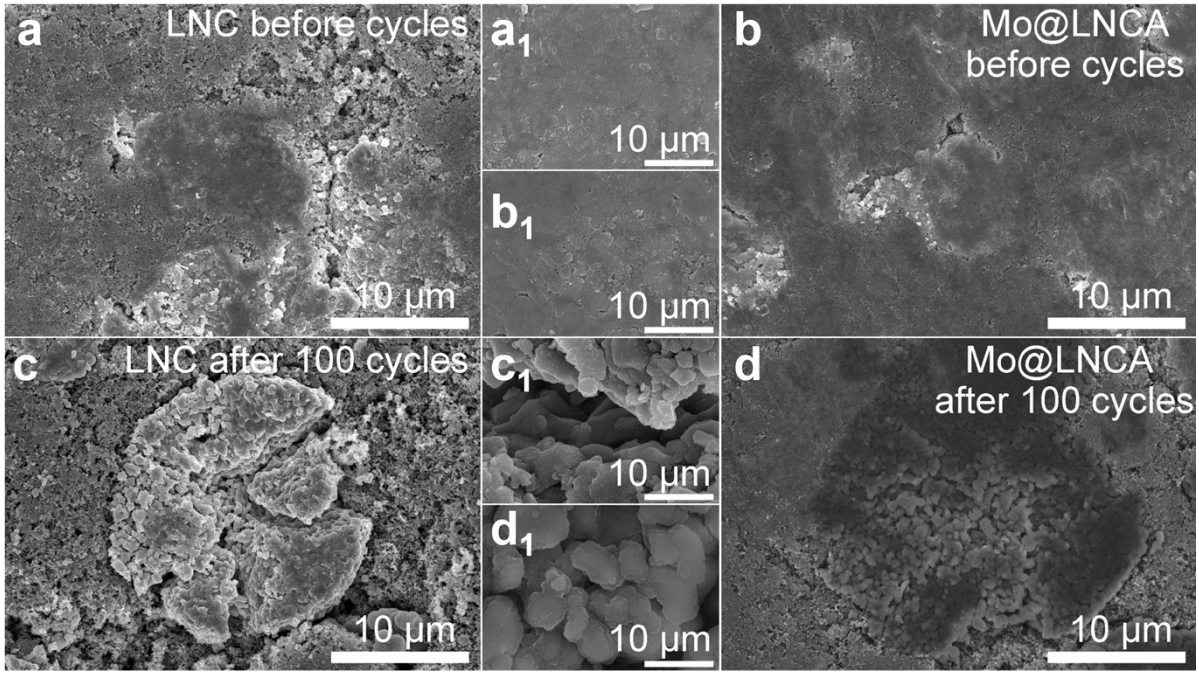

Fig. S15. SEM images of a) LNC and b) Mo@LNCA before and after 100 cycles.

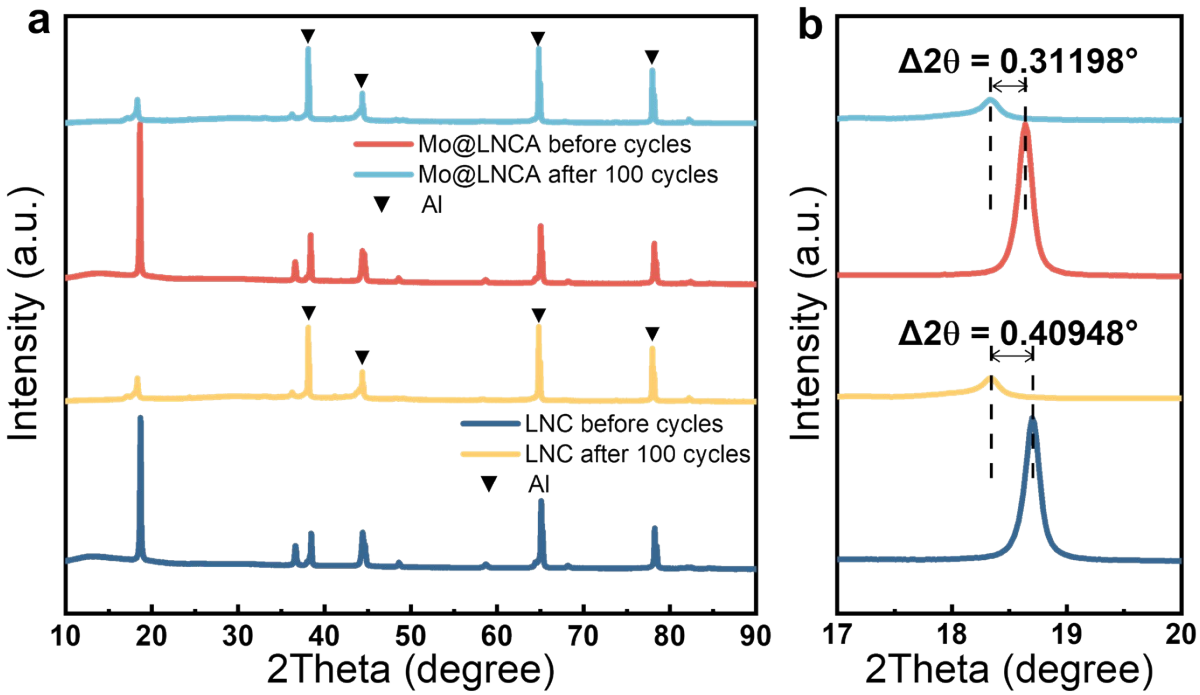

Fig. S16. a) XRD patterns of the LNC and Mo@LNCA pole flake with enlarged views of b) (003) peaks before and after 100 cycles.

Table S1. The Rietveld refinement data for LNC, LNCA and Mo@LNCA

Samples	a=b (Å)	c (Å)	c/a	V (Å^3)	I003/I104	R_{wp} (%)	R_p (%)	Ni^{2+}	Li^+	Ni^{2+} in Li^+ Layer (%)
LNC	2.87302	14.1864	4.93780	101.16	2.05798	1.85	1.30	0.0430	0.9570	4.49%
LNCA	2.86723	14.1925	4.94988	100.92	1.93735	1.79	1.24	0.0241	0.9759	2.47%
Mo@LNCA	2.87407	14.2154	4.94609	101.21	1.96181	1.70	1.16	0.0125	0.9875	1.27%

Table S2. Normalized relative atomic ratio of transition metals obtained by XPS etching spectroscopy.

Transition metals atomic fraction (%)	Etching time (s)					
	0	30	60	90	120	150
Ni	80.9049	85.2246	88.3344	88.7702	88.6035	87.8454
Co	7.7844	7.8351	6.6522	6.4465	6.3779	6.4660
Al	5.4302	4.7950	3.6576	3.5802	4.0135	4.6563
Mo	5.8805	2.1453	1.3558	1.2031	1.0051	1.0323

Table S3. Migration energy barrier of Al atoms in transition metal layer of the Mo@LNCA.

Ni layer	Ralative energy (eV)
0	0
1	-4.15015
2	-4.22485
3	-4.08925